53rd AIAA/ASME/ASCE/AHS/ASC Structures, Structural Dynamics and Materials Conference
20th AI
23 - 26 April 2012, Honolulu, Hawaii

AIAA 2012-1537

Investigation of progressive damage and fracture in laminated composites using the smeared crack approach

Christian Heinrich* and Anthony M. Waas†

University of Michigan, Ann Arbor, Michigan, 48109, USA

The smeared crack approach (SCA) is revisited to describe post-peak softening in laminated composite materials. First, predictions of the SCA are compared against linear elastic fracture mechanics (LEFM) based predictions for the debonding of an adhesively bonded double cantilever beam. A sensitivity analysis is performed to establish the influence of element size and cohesive strength on the load-deflection curves. The SCA is further validated by studying the in-plane fracture of a laminated composite. In doing so, issues related to mesh size and their effects (or non-effects) are discussed and compared against other predictive computational techniques. Finally, the SCA is specialized to orthotropic materials. The application of the SCA is demonstrated for failure mechanics of the open hole tension test.

Nomenclature

a	Crack length
b	Width of cantilever beam
$\boldsymbol{D}^{co}$	Continuum stiffness
$\boldsymbol{D}^{cr}$	Unloading stiffness
$\boldsymbol{D}^{da}$	Damping matrix
E	Elastic modulus
E^{cr}	Crack stiffness normal to the crack surface
E_f^{cr}	Crack stiffness in the fiber direction
E_m^{cr}	Crack stiffness perpendicular to the fiber direction (in the matrix direction)
G_{IC}	Strain energy release rate
G^{cr}	Crack shear stiffness tangential to the crack surface
G_m^{cr}	Crack shear stiffness in the matrix
I	Area moment of inertia
N	Transformation from global to crack coordinate system
$\boldsymbol{e}^{cr}$	Crack strain in crack coordinate systems
h	Characteristic length
$\boldsymbol{s}^{cr}$	Crack stress in crack coordinate system
Δt	Time increment
$\boldsymbol{\varepsilon}$	Total strain
$\boldsymbol{\varepsilon}^{co}$	Continuum strain
$\boldsymbol{\varepsilon}^{cr}$	Crack strain
$\dot{\boldsymbol{\varepsilon}}^{cr}$	Crack strain rate
ε_f^{cr}	Crack strain in the fiber direction
ε_m^{cr}	Crack strain perpendicular to the fiber direction (in the matrix direction)

*Post Doctoral Research Fellow, Department of Aerospace Engineering, 1320 Beal Avenue, 48109 Ann Arbor, MI, Student Member AIAA

†Felix Pawlowski Collegiate Professor of Aerospace Engineering, Department of Aerospace Engineering, 1320 Beal Avenue, 48109 Ann Arbor, MI, Fellow AIAA

ε^{cr}_{norm} Crack strain normal to the crack surface
$\boldsymbol{\varepsilon}^{el}$ Elastic strain
$\boldsymbol{\varepsilon}^{pl}$ Plastic strain
γ^{cr}_{m} Crack shear strain in the matrix
γ^{cr}_{t1} Crack strain tangential to the crack surface
γ^{cr}_{t2} Crack strain tangential to the crack surface
η Damping coefficient
$\boldsymbol{\sigma}$ Stress
σ^{cr}_{f} Crack stress in the fiber direction
σ^{cr}_{m} Crack stress perpendicular to the fiber direction (in the matrix direction)
σ^{cr}_{norm} Crack stress normal to the crack surface
τ^{cr}_{t1} Crack stress tangential to the crack surface
τ^{cr}_{t2} Crack stress tangential to the crack surface
τ^{cr}_{m} Shear crack stress in the matrix

I. Introduction

Validated computational methods are required to ensure Structural Integrity and Damage Tolerance (SIDT) of laminated composites used in primary aerospace structures. These computational methods serve to duplicate and drastically reduce the number of tests associated with several layers in the building-block approach to aerospace material qualification, leading to cost reduction. Virtual testing and integrated computational engineering of composite structures is now an active field of research and development in the quest to certify composite structures for insertion into various aerospace structural platforms. For SIDT to be successful in a virtual platform, the various mechanisms that govern the onset and progression of fracture and damage needs in laminated composites to be understood across disparate length scales and modeled efficiently using advanced, validated, computational methods. There are a variety of theories and numerical implementations with respect to the modeling of progressive damage and failure in solids. These studies were initially focussed on modeling the failure of brittle concrete. A comprehensive discussion of the theories, and to some degree their numerical implementation, is available in the text-book by Bažant and Cedolin.[1] In this paper, the smeared crack approach (SCA), first conceived by Bazant and Oh[2] as the crack band model, and later refined by Rots,[3] will be adopted to investigate delamination failure in composite laminates. When properly implemented it promises a large degree of objectivity with respect to numerical discretization while requiring little or no modification to standard, commercial finite element codes. This latter aspect is of great concern to practising engineers in industry who are concerned with virtual testing related to SIDT.

II. Summary of failure models

The modeling of failure in the context of the finite element method (FEM) can be roughly divided into two categories: discrete and continuum approaches. In the discrete approach, cracks are modeled as strong discontinuities. Examples are the virtual crack closure technique (VCCT),[4] cohesive zone models (CZM)[5] and discrete cohesive zone models (DCZM).[6] A drawback of these methods is the need to specify the crack path a-priori. This is not the case for the variational multiscale cohesive method-VMCM,[7] and the extended finite element method (X-FEM).[8] In these methods, the crack path may be arbitrary. However calculations of the X-FEM method are time consuming, which is in part due to the change in sparsity pattern associated with the FEM matrices, as additional nodes and degrees of freedom get activated as the crack progresses. This point of concern was resolved by VMCM where the degrees of freedom associated with the cohesive law are condensed out and solved for at the element level, leading to a reduction in computational cost, particularly as the problem complexity grows (for instance, as the number of cracks to be modeled increases, the VMCM computational cost does not increase, whereas the XFEM cost does increase, see[9]). For all discrete methods, the prediction of crack direction and crack tracking is a difficult task in 3D implementations.[10] As all of these approaches are concerned with the crack as a strong discontinuity with a well defined boundary, no further attention need to be given to the continuum representation of material next to the crack or in other parts of the structure. Here standard procedures of continuum mechanics can be used to model the material. Computational approaches based on the strong discontinuity formulation, in general, are mesh objective,

differing in cost between the different implementations (for example, VMCM vs. X-FEM, see[9]).

Compared to explicit modeling of cracks (as in the strong discontinuity approach), continuum damage mechanics (CDM) approaches[11–14] model the *effect* of cracks on progressive failure much more efficiently, and thus these methods may be better suited for integrated computational frameworks for the building-block approach. However care needs to be taken to avoid spurious mesh dependence. In CDM approaches, cracks are not modeled explicitly, instead their effects on mechanical response are modeled. This is usually due to the fact that large amounts of small cracks and voids are distributed over a finite volume, and it would be too exhaustive to model them individually. This type of behavior can be found in concrete as well as in the matrix material of composites,[15] but also in some metals. A major advantage of CDM (compared to plasticity theory based approaches) is its ability to capture post-peak softening.[12,13] With CDM, two stages can be distinguished - pre-peak and post-peak response. Both are sometimes referred to as "softening", but with different connotations. Before the peak load is reached, the secant stiffness (in the case of pure damage) or the unloading stiffness (in the case of damage combined with a permanent set/ plasticity) decreases. Here the softening refers to a reduction of stiffness. However the tangent stiffness remains positive. After the peak load is reached, the secant and the tangent stiffness are negative and the load decreases with increasing strain. This is also termed softening (especially in the civil engineering community that deals with concrete). Only the second type of softening is of concern in the context of mesh objectivity. Once the tangent stiffness turns negative, a material description in terms of stress and strain is no longer objective. Failure will localize into a zone, distinguished by a *characteristic length scale*. If classical continuum mechanics is used in the context of FEM, the only characteristic length scale present in the model is the element size. Therefore localization will take place within one element, regardless of its size. Consequently the energy dissipated during the failure process will be a function of element size and zero dissipation will occur in the limit of vanishing element size. This behavior is not associated with errors due to numerical discretization, but of the underlying mathematical description associated with capturing post-peak response.[1] To restore mesh objectivity, a characteristic length scale needs to be incorporated into the underlying continuum equations. Techniques that adopt this, include non-local[16] and gradient based theories,[17–19] and Cosserat-Continua.[20] While these approaches are academically quite appealing, the correct (experimental) determination of the characteristic length scale remains an area of ongoing debate and discussion.

Alternatively, instead of using a material description based on stress and strain, one based on stress and displacement can be employed to restore objectivity. The idea here is to demarcate material in the pre-peak (positive definite tangent stiffness) as being governed by classical continuum theories and those in the post-peak (negative definite tangent stiffness) as being governed by traction-separation laws, and including a *characteristic length scale*. This is the same approach that is used in the DCZM, where the crack on-set and progression is governed through a traction-separation law. The SCA,[3] crack band approach[2] and weak discontinuity approach[21] all refer to such a transition from a strain based to a displacement based description. These approaches can be interpreted in two ways. The first refers to the original motivation of damage mechanics: during the localization of the material many distributed micro cracks are present in a crack band of finite size. Their combined effect causes a globally observed softening. A second interpretation is the hiding of a discrete crack inside a a finite element, representing a finite volume of material. This last viewpoint emphasizes the need to transition from a continuum to a non-continuum description when the material enters a non-positive definite tangent stiffness.

III. Governing equations of smeared crack approach

Two slightly different approaches will be presented in the following. A three dimensional model for isotropic materials will be introduced first. Such a model is useful to describe the crack progression in the matrix material in a composite. Then, a 2D orthotropic SCA model is presented. It can be used to model the crack and damage progression within the layers of a laminate.

A. 3D isotropic model

In the following, the SCA approach similar to the one by Rots et al.,[3] is extended to damage and failure in orthotropic materials, so that progressive damage development and failure of composite laminates can be tackled in a mesh objective manner. In the pre-peak regime, standard continuum descriptions of the material are assumed to hold. In the post peak regime, it is assumed that the total strain ε may be split up

into a continuum part ε^{co} and a crack part ε^{cr}

$$\varepsilon = \varepsilon^{co} + \varepsilon^{cr} \tag{1}$$

If a plastic model, such as Hills anisotropic plasticity theory, is used, the continuum strain is additionally decomposed into elastic and plastic contributions.

$$\boldsymbol{\varepsilon} = \boldsymbol{\varepsilon}^{el} + \boldsymbol{\varepsilon}^{pl} + \boldsymbol{\varepsilon}^{cr} \tag{2}$$

All the quantities are given in the global coordinate system. The crack strains can be transformed from the global to the local coordinate system via the transformation law $\boldsymbol{N}$, as

$$\boldsymbol{\varepsilon}^{cr} = \boldsymbol{N}\boldsymbol{e}^{cr} = \boldsymbol{N} \begin{bmatrix} \varepsilon^{cr}_{norm} \\ \gamma^{cr}_{t1} \\ \gamma^{cr}_{t2} \end{bmatrix} \tag{3}$$

Here ε^{cr}_{norm} is the crack component normal to the crack and γ^{c}_{t1} and γ_{t2} are the components tangential to the crack surface. In a similar fashion, the global stress state $\boldsymbol{\sigma}$ can be transformed to yield the tractions at the crack interface $\boldsymbol{s}^{cr}$

$$\boldsymbol{s}^{cr} = \begin{bmatrix} \sigma^{cr}_{norm} \\ \tau^{cr}_{t1} \\ \tau^{cr}_{t2} \end{bmatrix} = \boldsymbol{N}^T\boldsymbol{\sigma} \tag{4}$$

Various criteria to calculate the transformation matrix $\boldsymbol{N}$ are possible. If the Rankine criterion of maximum principle stress is used to determine crack onset, it is convenient to use the principle stress directions as the crack directions. The tractions at the crack interface are related to the crack strains trough the secant stiffness matrix D^{cr3} and a damping matrix by

$$\boldsymbol{s}^{cr} = \boldsymbol{D}^{cr}\boldsymbol{e}^{cr} + \boldsymbol{D}^{da}\dot{\boldsymbol{e}}^{cr} \tag{5}$$

The damping matrix makes the crack progression a time-dependent property. It can also be used to smoothen the numerical solution scheme. Any numerical solution scheme involves a discrete time step. The crack strain rate is accordingly approximated with finite differences.

$$\dot{\boldsymbol{e}}^{cr} \approx \frac{\boldsymbol{e}^{cr}(t+\Delta t) - \boldsymbol{e}^{cr}(t)}{\Delta t} = \frac{\boldsymbol{e}^{cr} - \boldsymbol{e}^{cr}_{old}}{\Delta t} \tag{6}$$

The crack stress can finally be expressed as

$$\boldsymbol{s}^{cr} = \boldsymbol{D}^{cr}\boldsymbol{e}^{cr} + \frac{1}{\Delta t}\boldsymbol{D}^{da}\boldsymbol{e}^{cr} - \frac{1}{\Delta t}\boldsymbol{D}^{da}\boldsymbol{e}^{cr}_{old} \tag{7}$$

The expanded equation (7) yields

$$\begin{aligned} \begin{bmatrix} \sigma^{cr}_{norm} \\ \tau^{cr}_{t1} \\ \tau^{cr}_{t2} \end{bmatrix} &= \begin{bmatrix} E^{cr}(\varepsilon^{cr}_{norm}) & 0 & 0 \\ 0 & G^{cr}(\varepsilon^{cr}_{norm}) & 0 \\ 0 & 0 & G^{cr}(\varepsilon^{cr}_{norm}) \end{bmatrix} \begin{bmatrix} h\cdot\varepsilon^{cr}_{norm} \\ h\cdot\gamma^{cr}_{t1} \\ h\cdot\gamma^{cr}_{t2} \end{bmatrix} \\ &+ \frac{1}{\Delta t}\begin{bmatrix} \eta & 0 & 0 \\ 0 & \eta & 0 \\ 0 & 0 & \eta \end{bmatrix} \begin{bmatrix} h\cdot\varepsilon^{cr}_{norm} \\ h\cdot\gamma^{cr}_{t1} \\ h\cdot\gamma^{cr}_{t2} \end{bmatrix} - \frac{1}{\Delta t}\begin{bmatrix} \eta & 0 & 0 \\ 0 & \eta & 0 \\ 0 & 0 & \eta \end{bmatrix} \begin{bmatrix} h\cdot\varepsilon^{cr}_{norm} \\ h\cdot\gamma^{cr}_{t1} \\ h\cdot\gamma^{cr}_{t2} \end{bmatrix}_{old} \end{aligned} \tag{8}$$

where σ^{norm} is the normal traction across the crack surface and $E_{cr}(\varepsilon^{cr}_{norm})$ is the tensile secant stiffness across the crack surface. The crack shear stiffness G^{cr} is given here as a function of the normal crack opening $\varepsilon^{crack}_{norm}$ only. This implies that locally the crack opening is purely mode I dominated. It is also possible make the shear stiffness a function of the crack shear opening γ^{cr}_{t}. However this might be difficult to justify on a micromechanical basis.
The constitutive relation for the continuum is given by

$$\boldsymbol{\sigma} = \boldsymbol{D}^{co}\boldsymbol{\varepsilon}^{el}, \tag{9}$$

where $\boldsymbol{D}^{co}$ is the secant stiffness of the continuum. Combining all equations yields an implicit relation between the crack strain and the total elastic strain.

$$\boldsymbol{e}^{cr} = \left[\boldsymbol{D}^{cr}(\boldsymbol{e}^{cr}) + \boldsymbol{N}^T\boldsymbol{D}^{co}\boldsymbol{N} + \frac{1}{\Delta t}\boldsymbol{D}^{da}\right]^{-1}\left[\boldsymbol{N}^T\boldsymbol{D}^{co}\boldsymbol{\varepsilon}^{elcr} + \frac{1}{\Delta t}\boldsymbol{D}^{da}\boldsymbol{e}^{cr}_{old}\right] \tag{10}$$

Finally, the relation between total stress and total strain in the post peak regime are found as

$$\begin{aligned}\boldsymbol{\sigma} &= \left[\boldsymbol{D}^{co} - \boldsymbol{D}^{co}\boldsymbol{N}\left(\boldsymbol{D}^{cr} + \boldsymbol{N}^T\boldsymbol{D}^{co}\boldsymbol{N} + \frac{1}{\Delta t}\boldsymbol{D}^{da}\right)^{-1}\boldsymbol{N}^T\boldsymbol{D}^{co}\right]\boldsymbol{\varepsilon}^{elcr} \\ &- \frac{1}{\Delta t}\left[\boldsymbol{D}^{cr}(\boldsymbol{e}^{cr}) + \boldsymbol{N}^T\boldsymbol{D}^{co}\boldsymbol{N} + \frac{1}{\Delta t}\boldsymbol{D}^{da}\right]^{-1}\boldsymbol{D}^{da}\boldsymbol{e}^{cr}_{old}\end{aligned} \tag{11}$$

The *total* stress-strain description, such as equation (11), which is more suited for large time increments during reversed loading, is pursued here. It has been noted that the incremental approach can lead to a deviation from the prescribed traction-separation law, if the strain increments are too large.[22] An analogy to this behavior might be found in the incremental theory of plasticity. When an explicit integration scheme of the governing equations is used, the equivalent stress can deviate from the yield surface. This behavior led to the emergence of various return mapping schemes, which enforces that the stress at the end of an increment does not exceed the yield stress. In the same manner, eq (11) ensures that the stress at the end of an increment is in accordance with the traction-separation law.

Due to the requirement for the crack stresses to trace the traction-separation law, eq. (10) is a (highly) non-linear equation for the crack strain. It is solved via Newton's Method by defining a function that is to be minimized

$$\boldsymbol{f}(\boldsymbol{e}^{cr}) = \left[\boldsymbol{D}^{cr}(\boldsymbol{e}^{cr}) + \boldsymbol{N}^T\boldsymbol{D}^{co}\boldsymbol{N} + \frac{1}{\Delta t}\boldsymbol{D}^{da}\right]\boldsymbol{e}^{cr} - \boldsymbol{N}^T\boldsymbol{D}^{co}\boldsymbol{\varepsilon} - \frac{1}{\Delta t}\boldsymbol{D}^{da}\boldsymbol{e}^{cr}_{old} = 0. \tag{12}$$

The crack strain is then found iteratively, where successive iterations are given by

$$[\boldsymbol{e}^{cr}]^{(k+1)} = [\boldsymbol{e}^{cr}]^{(k)} - \left[\frac{\mathrm{d}\boldsymbol{f}}{\mathrm{d}\boldsymbol{e}^{cr}}\right]^{-1}\boldsymbol{f}(\boldsymbol{e}^{cr}) \tag{13}$$

Once the consistent crack strains are found, eq. 11 can be used to find the stress at the end of an increment.

The strain values in equation (8) are multiplied with a characteristic length scale, to transform it into a true traction-separation law. The characteristic length is obtained by requiring that the energy dissipation during fracture of a continuum element of a given size has to be the same as a cohesive element of the same size, described in terms of a traction-separation law. Typically the size of the element projected onto the crack normal is used, as shown in figure 1.

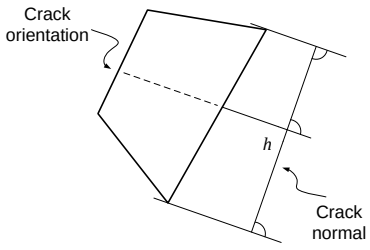

Figure 1: Characteristic element length from projection of crack normal

Here it should be noted that the critical strain energy release rate is the integral of the traction over the separation (see figure 2), and is defined as,

$$G_{IC} = \int_0^{\delta_{ult}} \sigma \mathrm{d}\delta \tag{14}$$

$$= \int_0^{\varepsilon^{cr}_{ult}} \sigma h \mathrm{d}\varepsilon^{cr} \tag{15}$$

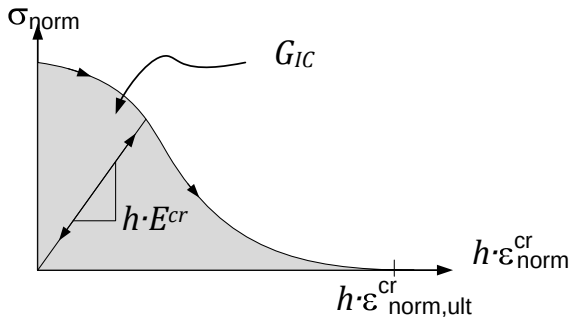

Figure 2: Crack interface stiffness

In practical applications, the secant stiffness matrix is chosen such the tractions will follow the traction separation law as shown in figure 3 exactly. To determine the secant stiffness, the current crack strain is found from equation (10) for a given current total strain. Then, the secant modulus can be found from the traction-separation law. As equation (10) is given in terms of total stress and total strain, some additional provisions to prevent crack "healing" are required. Specifically it has to be ensured that $\dot{E}^{cr} < 0$ and $\dot{G}^{cr} < 0$. In practice this is done by storing the previous and the current secant stiffness in memory. During a possible unloading the crack opening decreases. This leads to a decrease in crack strain and an increase in secant crack stiffness. In this case, the old crack secant stiffness is used. As a result the crack strain follows on a straight line to the origin during an unloading phase. In a subsequent loading phase, the traction will increase linearly with the crack strain until the envelope given by the original traction-separation law is reached and further softening occurs. Repeated loading and unloading behavior is also shown in figure 3.

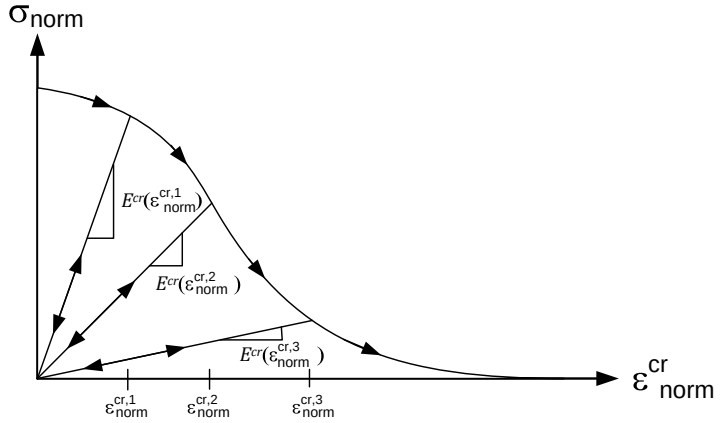

Figure 3: Evolution of crack interface stiffness during repeated loading and unloading

The softening of individual elements will cause convergence issues in a static, implicit analysis, because unless provisions are made for local snap-back (i.e. to accommodate local, unstable equilibrium paths; a remedy is to use an arc-length solver, such as the Riks method in ABAQUS. Further details are given in[23]),

the solution will diverge. In these instances, an explicit scheme has an advantage, however these schemes are time intensive due to lack of unconditional stability. An implicit dynamics solution procedure, on the other hand, is a compromise, and has been used in conjunction with the commercial finite element code ABAQUS[24] for the results presented in this paper.

B. 2D orthotropic model

The derivation for the 2 dimensional SCA model for an orthotropic model that is specifically tailored for composite laminae are described next. For fiber reinforced lamina, the crack direction is not calculated as a function of the stress field. Instead it lines up with the fibers of a laminate, since fiber/matrix splitting is energetically more favorable that fiber breaking, for cracks that traverse across a lamina. This choice of crack direction is physically motivated and is not a restriction of the SCA method pursued here, as will be evident. Therefore the direction of crack progression is not calculated from the current stress field, but the possible failure directions are instead fixed. Figure 4 shows the possible failure modes. They are: (a) Mode I crack opening perpendicular to the fiber direction ("fiber brakeage"), (b) Mode I crack opening parallel to the fiber direction and (c) Mode II crack opening/ sliding parallel to the fiber direction. Failure mode (a) is dominated by fiber strength and fiber breaking toughness, while mode (b) and (c) are dominated by the matrix strength and matrix toughness. Due to the significantly higher strength of the fiber failure modes, modes (b) and (c) can be expected to be observed in most cases. This will be further illustrated in the results section.

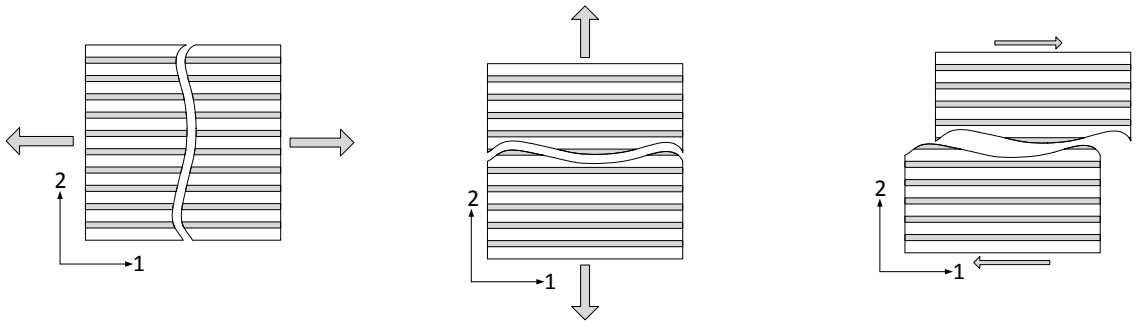

(a) Mode I fracture perpendicular to the fiber direction

(b) Mode I fracture parallel to the fiber direction

(c) Mode II fracture parallel to the fiber direction

Figure 4: Fracture modes in a fibrous composite

With the fiber direction denoted by "1", and the crack planes fixed parallel and perpendicular to the fiber direction, no coordinate transformation between the global frame and the crack frame is necessary and the transformation matrix $\boldsymbol{N}$ is unity. Therefore eq (3) can be modified to be

$$\boldsymbol{\varepsilon}^{cr} = \boldsymbol{e}^{cr} = \begin{bmatrix} \varepsilon_f^{cr} \\ \varepsilon_m^{cr} \\ \gamma_m^{cr} \end{bmatrix} \tag{16}$$

Accordingly the stresses across the crack surfaces can be described by

$$\boldsymbol{\sigma}^{cr} = \boldsymbol{s}^{cr} = \begin{bmatrix} \sigma_f^{cr} \\ \sigma_m^{cr} \\ \tau_m^{cr} \end{bmatrix} \tag{17}$$

It should be noted, that eqs. (16) and (17) represent two orthogonal cracks in two dimensions. Therefore two direct strain and stress components can be found. However, it is assumed that all shear is due to pure sliding parallel to the fibers.

Next, the constitutive law across the crack surfaces will be stated. For clarity, damping terms will be neglected.

$$\boldsymbol{\sigma}^{cr} = \boldsymbol{D}^{cr}\boldsymbol{\varepsilon}^{cr} \tag{18}$$

or expanded

$$\begin{bmatrix} \sigma_f^{cr} \\ \sigma_m^{cr} \\ \tau_m^{cr} \end{bmatrix} = \begin{bmatrix} E_f^{cr}(\varepsilon_f^{cr}) & 0 & 0 \\ 0 & E_m^{cr}(\varepsilon_m^{cr}) & 0 \\ 0 & 0 & G_m^{cr}(\gamma_m^{cr}) \end{bmatrix} \begin{bmatrix} \varepsilon_f^{cr} \\ \varepsilon_m^{cr} \\ \gamma_m^{cr} \end{bmatrix} \tag{19}$$

Here the stiffness is coupled to the crack opening in the corresponding direction. Compared to eq (8), the stiffness terms in eq (19) evolve differently. This is due to the fact that multiple crack opening modes are considered simultaneously, which have different values for the fracture toughness. Next, the expression to find the fracture strain at the current time can be deduced from eq (10), by noting that $\boldsymbol{N} = I$ and by neglecting damping and any nonlinear behavior in the pre-crack stage to be

$$\boldsymbol{e}^{cr} = \left[\boldsymbol{D}^{cr}(\boldsymbol{e}^{cr}) + \boldsymbol{D}^{co}\right]^{-1} \boldsymbol{D}^{co}\boldsymbol{\varepsilon} \tag{20}$$

Finally the stress can be found from

$$\boldsymbol{\sigma} = \left[\boldsymbol{D}^{co} - \boldsymbol{D}^{co}\left(\boldsymbol{D}^{cr} + \boldsymbol{D}^{co}\right)^{-1} \boldsymbol{D}^{co}\right] \boldsymbol{\varepsilon}. \tag{21}$$

IV. Results

A. Double cantilever beam

1. Model

As a first boundary value problem, a double cantilever beam (DCB) model will be investigated. The geometry is summarized in figure 5 and table 2. The material properties of the adherend and the adhesive layer are given in table 1.

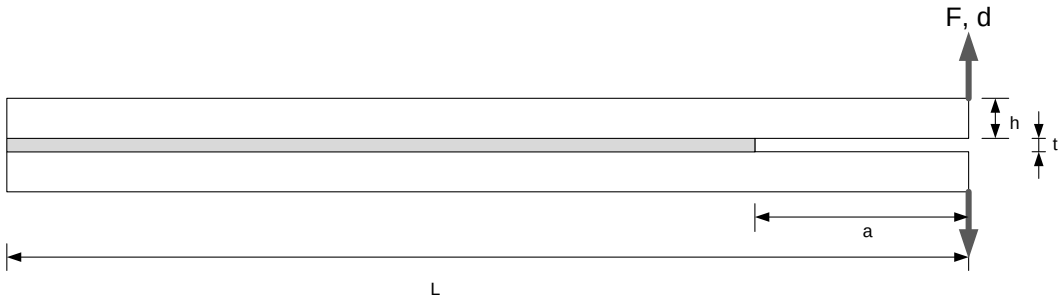

Figure 5: Geometry of DCB specimen

Adherent	
Elastic Modulus E	70 GPa
Poisson's ratio	0.3
Adhesive	
Mode I strain energy release rate	7.480 N/mm
Cohesive strength	503 MPa

Table 1: Material properties

Length L	100 mm
Height h	5 mm
Plane stress thickness b	1 mm
Initial crack length a	30 mm
Baseline crack thickness t	0.1 mm

Table 2: Geometry of DCB specimen

2. *Comparison with fracture mechanics*

A comparison of linear elastic fracture mechanics (LEFM) with the SCA is provided in figure 6. In the case of plane stress, the end load of a DCB specimen as a function of crack length is analytically evaluated as[25,26]

$$F = \frac{1}{a}\sqrt{EG_{IC}bI}. \tag{22}$$

where F is the applied end load, a is the crack length, I is the area moment of inertia and b is the beam width. Responses of the numerical and analytical solution are given in figure 6. They compare quite well. The LEFM solution shows a higher load for a smaller crack length. With increasing crack length, the SCA solution shows higher loads compared to the LEFM solution. This can be attributed to the incorporation of nonlinear geometric effects into the numerical simulation. The cantilever beams show an appreciable deflection which leads to a geometric stiffening effect. As the LEFM solution is based on small deflection beam theory, those effects are not represented in the LEFM solution.

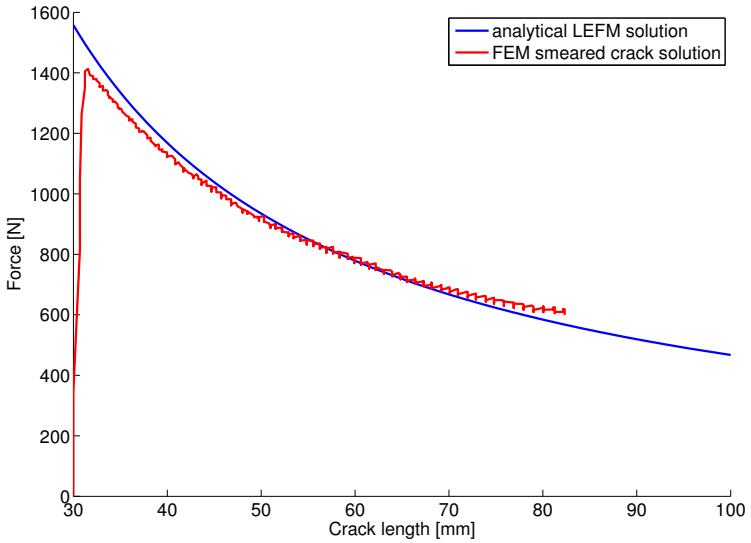

Figure 6: Comparison of the analytical and numerical solution of the end force as a function of crack length

3. *Influence of element number, fracture strength and crack band thickness*

Figure 7 shows the convergence of the load-displacement response of the DCB simulation with respect to the number of elements used in the adhesive layer. A clear oscillatory pattern is visible for a smaller number of elements along the crack direction. This is related to the integration scheme used to calculate nodal forces: stress and strain are evaluated at the integration points. When the stress at the integration point reaches a critical value, failure and softening is initiated. This softening influences the entire integration point volume. With increasing element number the amplitude and frequency due to failing integration points diminish. The solutions of 200, 400 and 800 elements are almost identical, suggesting that the solution is converged and is also *mesh objective*.

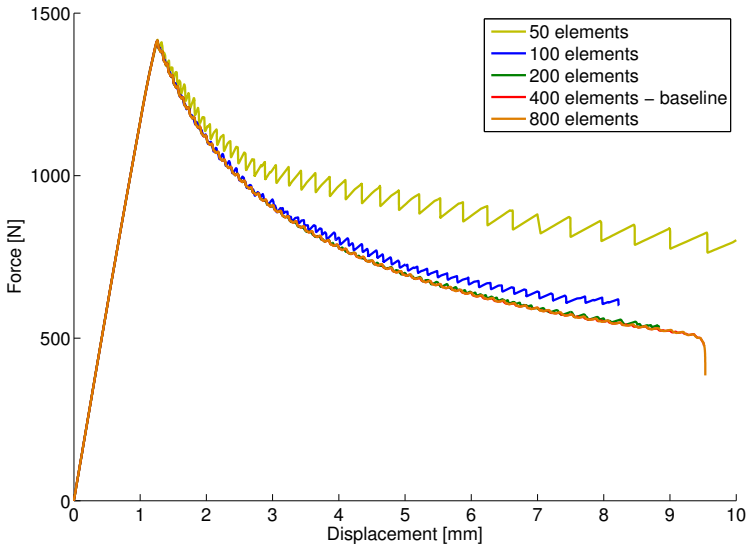

Figure 7: Convergence of the load-displacement curve with respect to number of elements

A valid criticism of using a two parameter model (cohesive strength and stain energy release rate) for a problem governed by linear elastic fracture mechanics (LEFM) is that the latter is only dependent on one material parameter (strain energy release rate or fracture toughness). The influence of the cohesive strength, from the LEFM point of view artificial, is depicted in figure 8. The curves for 1000 MPa, 503 MPa and 100 MPa show a clear convergence behavior: an increase in fracture strength yields a higher maximum load. Secondly the transition from the linear (loading) regime to the non-linear unloading and crack progression regime is sharper. Thirdly the numerically induced oscillations increase. The last two effects can be explained from considering that the fracture energy (per unit volume) is the area under the stress-fracture strain curve. As fracture energy is preserved, a decrease in fracture strength causes in increase in ultimate fracture strain. The implication of this is an increase in process zone size. In the case of high fracture stress only one or two elements fail at the same time. At lower fracture stress, the process zone is increased and several elements fail simultaneously. The result is a smoother force-deflection curve. In the cases of 10 MPa and 1 MPa fracture strength, the ultimate fracture strain, for the given strain energy release rate, is so large, that the process zone extends along the *entire specimen length* and even after an apparent separation of the two DCB arms a force is transmitted along the failure interface. Clearly, within the confines of the numerical model and LEFM, a desirable value of fracture strength is one that causes the process zone to extend over two or three elements at most. Thus, at this point, not just the unloading slope of the stress-strain law, but also fracture strength can be made a function of the mesh size. On the other hand, when looking beyond LEFM, it is physically hard to justify a different fracture strength than the one that would be measured from an independent test (such as the button-peel test, as described in,[27] or an appropriate tensile test. Therefore the reverse question can be posed as well: what is the maximum element size allowed, such that the the fracture process zone extends across at least two or three elements? When diverging from LEFM, the ultimate strain (or maximum opening/sliding) will govern the fracture process zone size or bridging zone size. It has been noted that laminated composites show a significant bridging in the wake of a crack.[7] A proper choice of cohesive strength and strain energy release rate will lead not only lead to the correct load-displacement prediction, but also to a correct prediction of the bridging zone, which is important to predict size effects.

In the context of fracture mechanics, the crack is infinitesimally thin and infinitesimally sharp. However standard finite elements are not capable of resolving such singularities. Figure 9 shows the influence of the crack (band) thickness on the load-displacement response of the DCB. A decrease in the crack band thickness causes a reduction in maximum load and a less sharp transition from the loading to the unloading/ crack progression regime. The reduction in maximum load can be attributed to the approach of a near singular stress field at the crack tip upon decrease of the crack band thickness. At the same time, the fracture energy is fixed. This means that a decrease in crack band size and element thickness increases the fracture ultimate

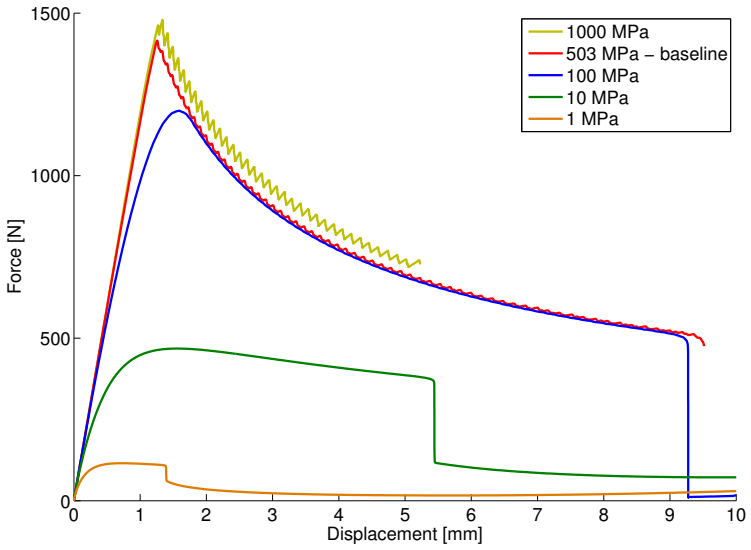

Figure 8: Influence of fracture stress/ strength on the load-displacement curve of DCB

strain (the ultimate "fracture displacement" is fixed). This causes a smoother transition from the loading to the unloading regime. When interpreting the results in figure 9 it should be kept in mind that the arms of the DCB setup have a thickness of 5 mm. Therefore the question of what constitutes an infinitesimally thin or sharp crack should be evaluated relative to other geometric dimensions.

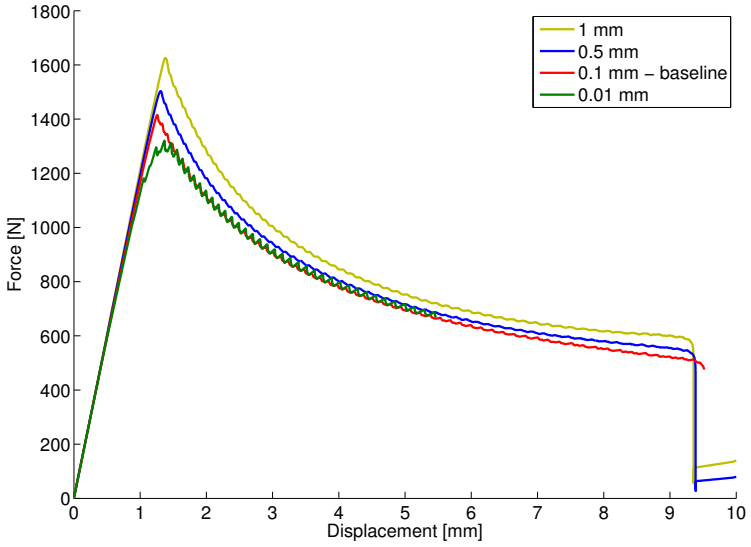

Figure 9: Influence of the crack band thickness on the load-displacement curve of DCB

4. DCB test of composite - Comparison with DCZM, VCCT and interface elements

Next, the SCA will be used to analyze the debonding of a laminated composite. Values are taken from Alfano and Crisfield,[28] who used an interface model to simulate an experiment. Xie and Waas[29] used the Discrete Cohesive Zone Element (DCZM) to do the same. They also provide a comparison with the virtual crack closure technique (VCCT).

The material properties are given in table 3.[28] The elastic modulus E, Poisson's ratio ν and layer thickness t of the adhesive are values that are not typically used in DCZM and similar approaches that use interface elements. Here they are necessary as the interface layer is represented by continuum elements.

Composite				
E_{11}(GPa)	$E_{22} = E_{33}$(GPa)	G_{12}(GPa)	$\nu_{12} = \nu_{13}$	ν_{23}
135.3	9.0	5.2	0.24	0.46
Interface				
G_{IC}(N/mm)	σ_f (MPa)	E(GPa)	ν	t(mm)
0.28	57.0	5.0	0.3	0.1

Table 3: Material properties for debonding of laminated composite beam

The comparison of the four models is given in figure 10. The smeared crack approach compares very well with the three other methods. The VCCT and DCZM method show an increase in stiffness at a crack length of about 8 mm which corresponds to the mathematical solution of a crack of that length. The smeared crack approach on the other hand shows a drop in load at this point. Here the crack has extended along the entire length of the specimen and the two beams are separated.

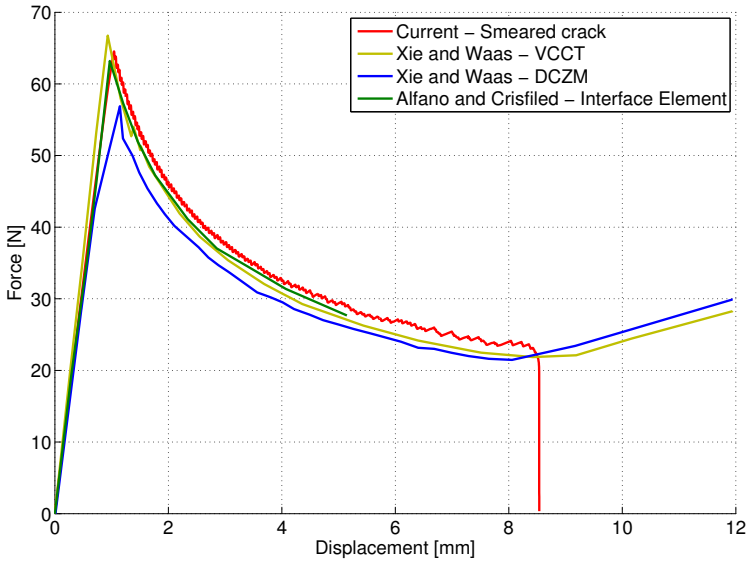

Figure 10: Comparison of smeared crack model with models that discretely represent the interface layer

B. Mesh convergence of single edge notch three-point bending specimen

To show convergence with respect to mesh size, consider an edge notch three-point bending (SETB) test. A typical test setup is described in figure 13. Three different mesh sizes have been chosen. The meshes are depicted in figure 11. The meshes consist of C3D6 wedge elements. The mesh sizes are 454, 1976 and 41140 elements. The results for the load-deflection response are very similar across all mesh sizes, as shown in figure 12. It can be noted that for the smallest mesh size, the initial elastic response is slightly stiffer due to a coarser discretization. The initial stiffness of the the second and third meshes are much closer. The different levels of discretization will also have an impact on the simulation of the crack progression, as smaller elements are better suited to resolve the stress field close to the crack tip.

C. Fracture of laminated composite

Next, the in-plane fracture of a laminated fiber reinforced composite was investigated using the example of a single edge notch three-point bending specimen. Rudraraju et al.[30] have investigated size effects using geometrically scaled specimens. Details of the experimental studies and numerical predictions using the

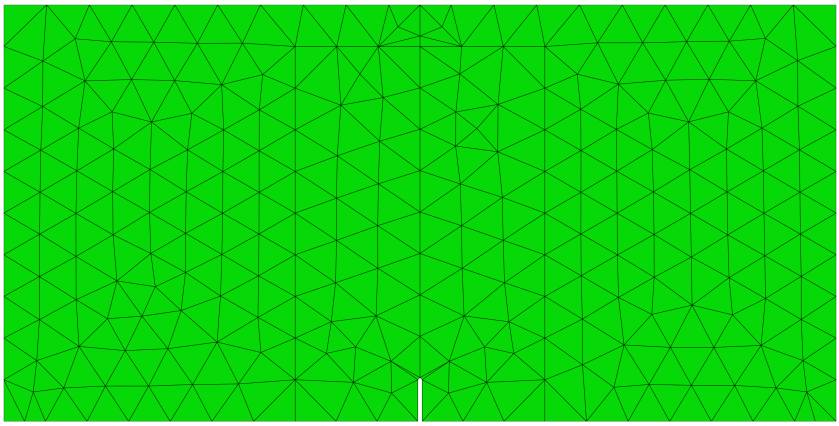

(a) 454 elements

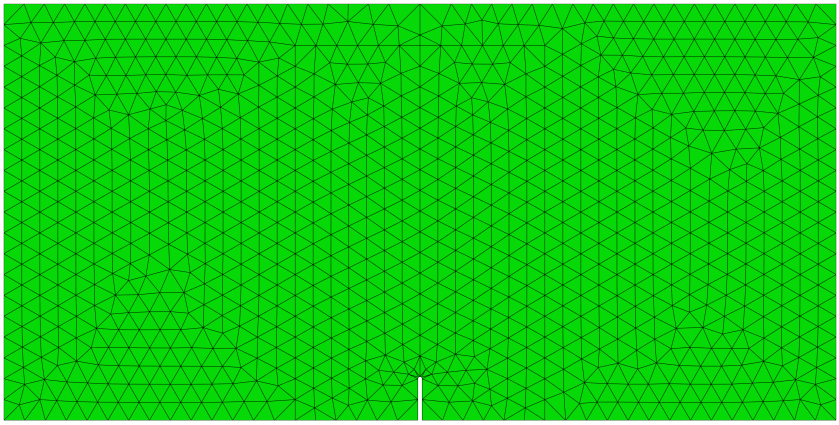

(b) 1976 elements

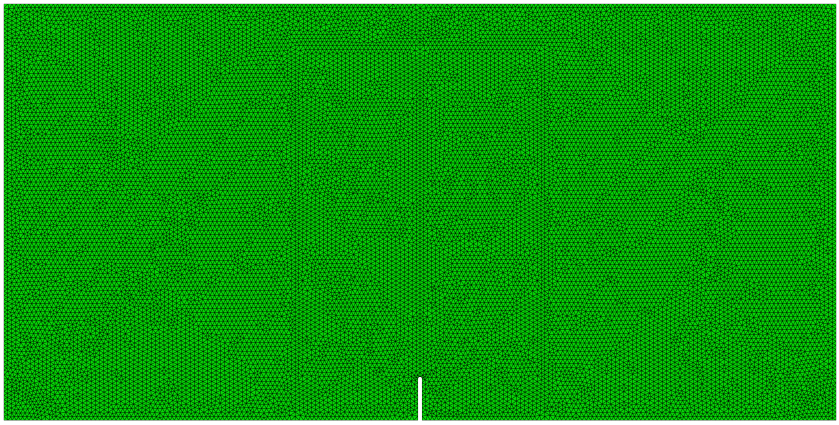

(c) 41140 elements

Figure 11: Three meshes used in SETB simulation

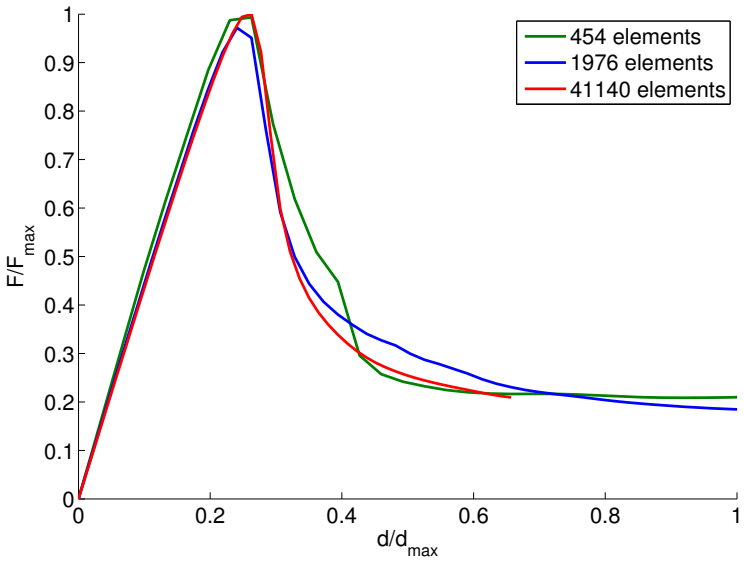

Figure 12: Comparison of the SETB response for different mesh sizes

VMCM are given in.[30] The geometry of the smallest size is depicted in figure 13. The laminate has a quasi-isotropic lay-up with an Elastic Modulus E=51.5 GPa and a Poisson's ratio ν=0.32.

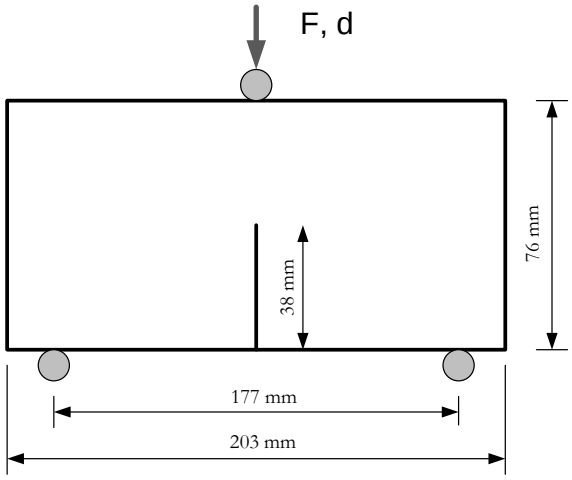

Figure 13: Geometry of single edge notch bending (SETB) specimen

Experimental results are matched well with the SCA predictions as shown in figure 14. It is noted that crack initiation takes place in the rising part of the load-deflection response. Further growth leads to a load maximum and beyond this maximum, the load drops with increasing crack advancement. The SCA predictions are shown to be mesh objective. Furthermore, both experimental and numerical simulations show a large bridging zone in the wake of the crack tip.

D. Open hole tension test of single layer laminate composite

The application of the the 2 dimensional orthotropic SCA is demonstrated using the open hole tension test of a single lamina, with the fiber direction oriented at various angles relative to the loading direction. The problem is described in figure 15. The hole diameter to width ratio is chosen to be 1/5. Additionally the loaded edges of the specimen are modeled as an isotropic soft material to reduce edge effects and to prevent

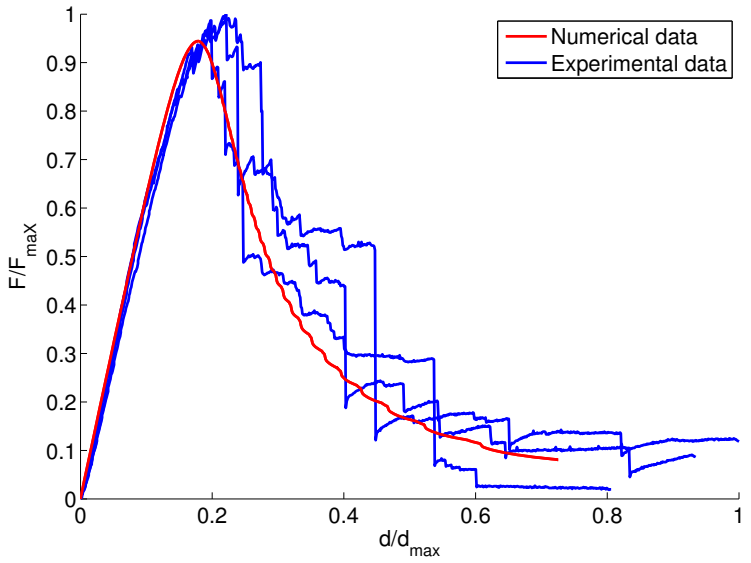

Figure 14: Normalized load-displacement response of SETB specimen

failure at the grips. The mesh of of the FE model is shown in figure 16. The mesh around the hole is finer than at the edges because of the stress gradients near the hole. The mesh consists of 15,425 reduced integration rectangular shell elements (S4R) in ABAQUS.

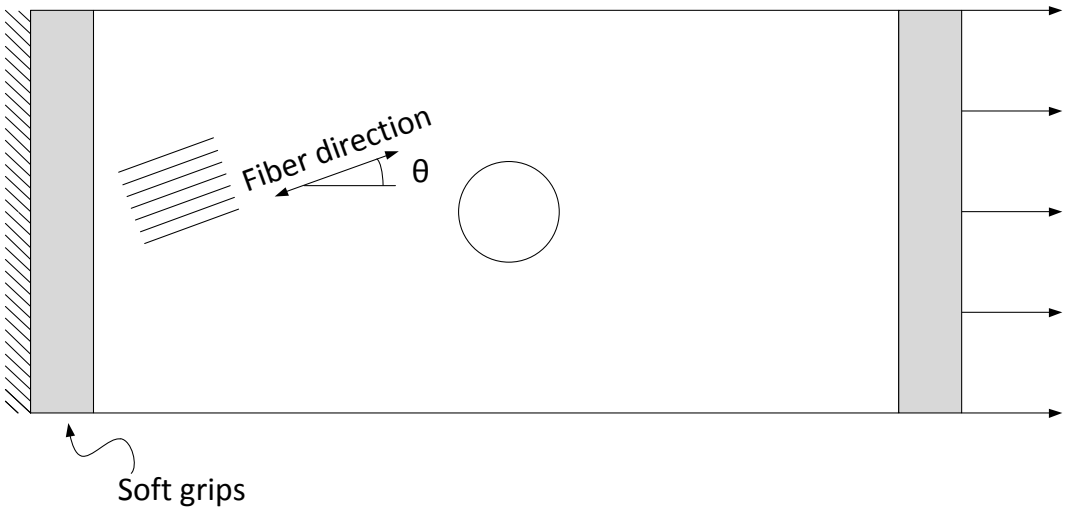

Figure 15: Single layer open hole test

Five different angles have been investigated: 0°, 5°, 45°, 85° and 90°. There is a clear shift in fracture modes noticeable. In the 0° and 5° case, the fracture strains for mode II are large, while the other fracture strains remain non existent. Therefore these cases are mode II dominated. On the other hand, the fracture strains for 45°, 85° and 90° are large for mode I parallel to the fibers ("matrix mode I"). This crack pattern is in agreement with the linear elastic stress distribution that can be used to draw conclusions about the nature of the fracture onset. In the case of 0° and 5°, the shear stress τ_{12} is dominant, while in the cases 45°, 85° and 90°, the stress component perpendicular, to the fibers σ_{22} is largest. In all cases, the crack direction lines up with the fiber direction. These results are encouraging and current work is aimed at incorporating the SCA in a laminate model for studying progressive failure and damage in multi-directional laminates.

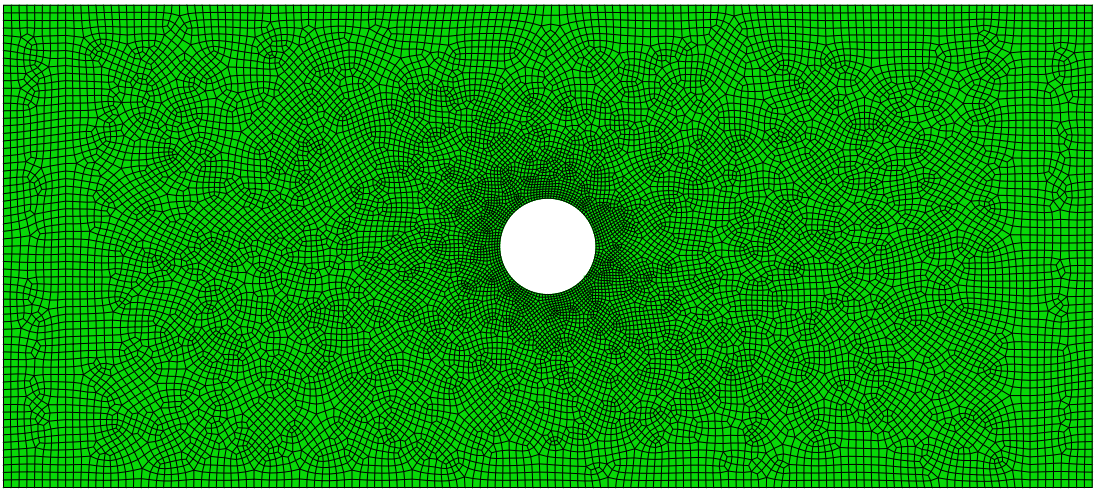

Figure 16: Setup of loading of single layer open hole laminate

V. Conclusion

The smeared crack approach (SCA) to capture post-peak softening, mesh objectively, in fracture and delamination of composites has been demonstrated. The loading stages of this technique can be interpreted in two ways. Prior to reaching an allowable stress, strain or a combined (in terms of stress and strain, in the form of $f(\sigma_{ij}, \epsilon_{ij}) = 0$), onset criterion, a classical continuum description is used. After reaching the onset criterion, the behavior has to be modeled through a description that departs from continuum mechanics. In the present work, we have used fracture energy and fracture strength, in opening and slides modes, as quantities that supply characteristic length scale/s, to describe the post-peak non-continuum response. The introduction of these characteristic length scales, which are based on physically measured properties that describe the failure of the composite material, leads to a mesh objective description that is *necessary* for predicting progressive damage and failure in composite structures. For the cases presented, the present approach leads to a high degree of objectivity with respect to mesh size used.

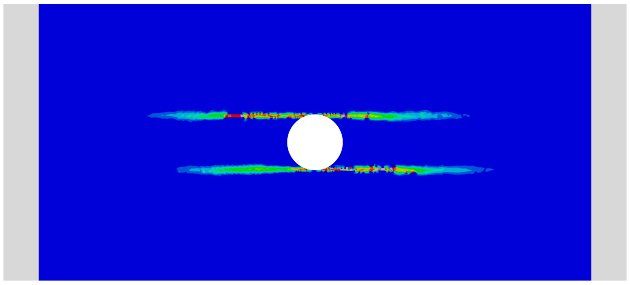

(a) 0°

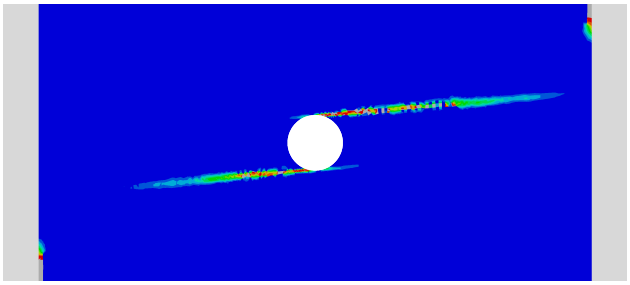

(b) 5°

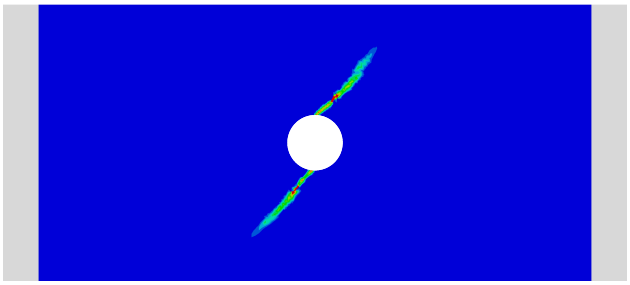

(c) 45°

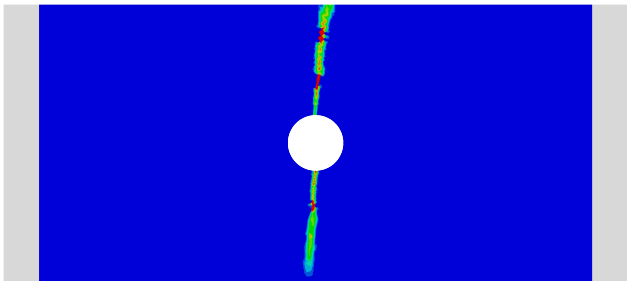

(d) 85°

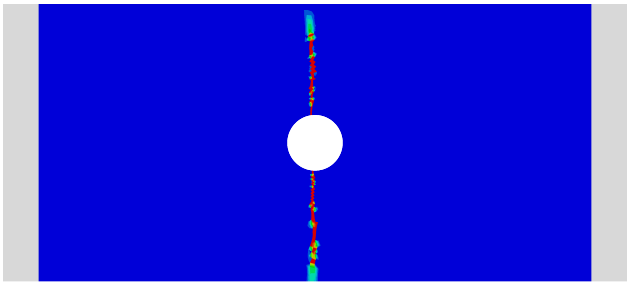

(e) 90°

Figure 17: Crack opening strain

Acknowledgments

This research was sponsored by the Boeing company and we are grateful for this support.

References

[1]Bažant, Z. and Cedolin, L., *Stability of structures: elastic, inelastic, fracture, and damage theories*, Courier Dover Publications, 2003.

[2]Bažant, Z. and Oh, B., "Crack band theory for fracture of concrete," *Materials and Structures*, Vol. 16, 1983, pp. 155–177, 10.1007/BF02486267.

[3]Rots, J., Nauta, P., Kuster, G., and Blaauwendraad, J., "Smeared Crack Approach and Fracture Localization in Concrete," *Heron*, Vol. 30, No. 1, 1985, pp. 1–48.

[4]Xie, D., Biggers, S. B., and Jr., "Strain energy release rate calculation for a moving delamination front of arbitrary shape based on the virtual crack closure technique. Part I: Formulation and validation," *Engineering Fracture Mechanics*, Vol. 73, No. 6, 2006, pp. 771 – 785.

[5]de Borst, R., "Numerical aspects of cohesive-zone models," *Engineering Fracture Mechanics*, Vol. 70, No. 14, 2003, pp. 1743 – 1757, Cohesive Models.

[6]Xie, D., Salvi, A. G., Waas, A. M., and Calicskan, A., "Discrete Cohesive Zone Model To Simulate Static Fracture In Carbon Fiber Textile Composites," *46th AIAA/ASME/ASCE/AHS/ASC Structures, Structural Dynamics & Materials Conference*, 2005.

[7]Rudraraju, S. S., Garikipati, A. S. K., and Waas, A. M., "Mixed mode in-plane fracture analysis of laminated fiber reinforced composites using the variational multiscale cohesive method," *51st AIAA/ASME/ASCE/AHS/ASC Structures, Structural Dynamics, and Materials Conference*, AIAA, April 2010, AIAA 2010-2860.

[8]Sukumar, N., Mos, N., Moran, B., and Belytschko, T., "Extended finite element method for three-dimensional crack modelling," *International Journal for Numerical Methods in Engineering*, Vol. 48, No. 11, 2000, pp. 1549–1570.

[9]Oliver, J., Huespe, A., and Snchez, P., "A comparative study on finite elements for capturing strong discontinuities: E-FEM vs X-FEM," *Computer Methods in Applied Mechanics and Engineering*, Vol. 195, No. 37-40, 2006, pp. 4732 – 4752, John H. Argyris Memorial Issue. Part I.

[10]Jger, P., Steinmann, P., and Kuhl, E., "Modeling three-dimensional crack propagationA comparison of crack path tracking strategies," *International Journal for Numerical Methods in Engineering*, Vol. 76, No. 9, 2008, pp. 1328–1352.

[11]Schapery, R., "Analysis of damage growth in particulate composites using a work potential," *Composites Engineering*, Vol. 1, No. 3, 1991, pp. 167 – 182.

[12]Lemaitre, J. and Desmorat, R., *Engineering Damage Mechanics: Ductile, Creep, Fatigue and Brittle Failures*, Springer-Verlag, 2005.

[13]Voyiadjis, G. Z. and Kattan, P. I., *Damage mechanics*, Talor & Francis, 2005.

[14]Basu, S., Waas, A. M., and Ambur, D. R., "Prediction of progressive failure in multidirectional composite laminated panels," *International Journal of Solids and Structures*, Vol. 44, No. 9, 2007, pp. 2648 – 2676.

[15]Talreja, R., "A Continuum Mechanics Characterization of Damage in Composite Materials," *Proceedings of the Royal Society of London. A. Mathematical and Physical Sciences*, Vol. 399, No. 1817, 1985, pp. 195–216.

[16]Pijaudier-Cabot, G. and Bažant, Z. P., "Nonlocal Damage Theory," *Journal of Engineering Mechanics*, Vol. 113, 1987, pp. 1512–1533.

[17]Askes, H., Pamin, J., and de Borst, R., "Dispersion analysis and element-free Galerkin solutions of second- and fourth-order gradient-enhanced damage models," *International Journal for Numerical Methods in Engineering*, Vol. 49, 2000.

[18]Askes, H. and Sluys, L. J., "Explicit and implicit gradient series in damage mechanics," *European Journal of Mechanics - A/Solids*, Vol. 21, No. 3, 2002, pp. 379 – 390.

[19]Pamin, J., Askes, H., and de Borst, R., "Two gradient plasticity theories discretized with the element-free Galerkin method," *Computer Methods in Applied Mechanics and Engineering*, Vol. 192, No. 20-21, 2003, pp. 2377 – 2403.

[20]de Borst, R., "Simulation of strain localization: A reappraisal of the cosserat continuum," *Engineering Computations*, Vol. 8, 1991, pp. 317–332.

[21]Oliver, J., Huespe, A. E., Samaniego, E., and Chaves, E. W. V., "Continuum approach to the numerical simulation of material failure in concrete," *International Journal for Numerical and Analytical Methods in Geomechanics*, Vol. 28, No. 7-8, 2004, pp. 609–632.

[22]Rots, J. G., *Computational modeling of concrete fracture*, Ph.D. thesis, Technical University Delft, September 1988.

[23]Crisfield, M. A., *Non-Linear Finite Element Analysis of Solids and Structures*, 1996.

[24]Simulia, *ABAQUS 6.10 manual*, Dassault Systems, 2010.

[25]Hertzberg, R. W., *Deformation and Fracture Mechanics of Engineering Materials*, John Wiley & Sons, Inc., 1996.

[26]Sanford, R., *Principles of Fracture Mechanics*, Peason Education, Inc., 2002.

[27]Sun, C., "Fracture of plastically-deforming, adhesively- bonded structures: experimental and numerical Studies," *PhD dissertation, University of Michigan, Ann Arbor, MI*, 2007.

[28]Alfano, G. and Crisfield, M. A., "Finite element interface models for the delamination analysis of laminated composites: mechanical and computational issues," *International Journal for Numerical Methods in Engineering*, Vol. 50, No. 7, 2001, pp. 1701–1736.

[29]Xie, D. and Waas, A. M., "Discrete cohesive zone model for mixed-mode fracture using finite element analysis," *Engineering Fracture Mechanics*, Vol. 73, No. 13, 2006, pp. 1783 – 1796.

[30]Rudraraju, S. S., Salvi, A., Garikipati, K., and Waas, A. M., "In-plane fracture of laminated fiber reinforced composites with varying fracture resistance: Experimental observations and numerical crack propagation simulations," *International Journal of Solids and Structures*, Vol. 47, No. 7-8, 2010, pp. 901 – 911.